Supporting Information

Boosting High Rate and Durability of Lithium-Sulfur Batteries via Bidirectional Catalyst of Polyoxometalate-Cyclodextrin Supramolecular Compound

Jian Song, Yuanyuan Jiang, Yizhong Lu*, Yundong Cao, Yuxi Zhang, Linlin Fan*, Hong Liu, and Guanggang Gao*

Collaborative Innovation Center of Metal Nanoclusters & Photo/Electro-Catalysis and Sensing

School of Materials Science and Engineering
University of Jinan
Jinan 250022, China.

*Corresponding authors
E-mail: mse_luyz@ujn.edu.cn (Yizhong Lu); mse_fanll@ujn.edu.cn (Linlin Fan); mse_gaogg@ujn.edu.cn (Guanggang Gao)

Table of Contents

Fig. S38. Raman spectra of pristine PW_{12}-CD and PW_{12}-CD modified separator with Nafion.

3. Supporting tables

Table S1. Electrochemical performance comparison of Li-S cell with PW_{12}-CD modified separator and other modified separators in recent literatures (sulfur loading ≤ 2 mg cm^{-2}).

Table S2. The reactions occurred on working and counter electrodes in Li_2S_6 symmetric cell.

Table S3. Electrochemical performance comparison of Li-S cell with PW_{12}-CD modified separator and other modified separators in recent literatures (sulfur loading ≥ 5 mg cm^{-2}).

1. Experimental Section

Materials characterization: The microstructures and elemental mappings were acquired using a scanning electron microscope (SEM, Zeiss Ultra 55 field-emission gun). X-ray diffraction (XRD) patterns were obtained using a Rigaku SmartLab 9KW instrument. X-ray photoelectron spectroscopy (XPS) measurements were conducted with a non-monochromatized Mg Kα X-ray excitation source on an ESCA Lab MKII X-ray photoelectron spectrometer. Fourier transform infrared spectroscopy (FTIR) data were collected using a NEXUS-870 spectrophotometer equipped with KBr pellets. Contact angles were measured using a POWEREACH JC2000D2G instrument. Ultraviolet-visible (UV-Vis) measurements were performed using a SHIMADZU UV-3600 spectrometer, covering the wavelength range of 200-600 nm. The sulfur content in the KB/S composite was determined under an N_2 atmosphere using thermogravimetric analysis (TGA) on a TA Instrument Q 600 Analyzer, with a heating rate of 10 ℃ min^{-1}. In-situ Raman spectroscopy was carried out on a Raman lithium-ion battery system (Beijing Scistar Technology Co., Ltd.), employing a Raman spectrometer (Labramis, Horiba Jobbin Yvon, Paris, France) with a wavelength of 532 nm. The specific surface area of samples was determined by the Brunauer-Emmett-Teller (BET) nitrogen adsorption/desorption method (Quadrasorb SI-MP, Quantachrome).

Preparation of PW_{12}-CD modified separators: PW_{12}-CD crystal was prepared according to the method previously reported with some modifications.[1] Specifically, 0.12 mmol $H_3PW_{12}O_{40}\cdot xH_2O$ and 0.36 mmol NaCl were dissolved in 12 mL ultra-pure water. Subsequently, HCl was added to the above solution and the pH was adjusted to 1. At room temperature, 0.13 mmol γ-CD was added under stirring. With vigorous stirring, adding 1.20 mmol $Co(NO_3)_2\cdot 6H_2O$ to the above solution until it reached a clear state. Finally, the obtained pink transparent solution was placed in an open vial and vaporized for crystallization at room temperature. PW_{12}-CD, Super P, and PVDF (in an 8:1:1 weight ratio) were finely ground with

NMP in an agate mortar to form a a mixed slurry. The mixed slurry was coated on one side of the PP separator by the doctor blade. Subsequently, the modified separators were dried at 50 ℃ for 24 h, then punched into a Ø20 mm circular membrane. CD and PW_{12} modified separators were prepared using the same method as above.

Preparation of sulfur cathode: The melt-diffusion method was used to infiltrate the appropriate amount sulfur into KB. The KB and S were uniformly mixed with a weight ratio of 3:7, and the resulted products were heated at 155 ℃ for 12 h under Ar atmosphere to obtain the KB/S composite.

Cell assembly and electrochemical measurement: For Li-S cells, the cathode was prepared by casting a paste that consisted of KB/S, Super P, and PVDF (mass ratio of 8:1:1) onto an aluminum foil. The coated electrodes were dried in a vacuum oven at 60 ℃ overnight and punched into a Ø10 mm circular membrane. The areal loading of active sulfur was 1.6 mg cm^{-2}. While the cathodes with high sulfur loading of 3.3, 4.6, 6.0 and 10.3 mg cm^{-2} were prepared by mixing KB/S, Super P, and LA133 (5 wt%) (mass ratio of 84:10:6). Lithium metal and Celgard 2500 PP were used as anode and separator, respectively. 1.0 M LiTFSI in DOL and DME (V/V = 1:1) with 2 wt% $LiNO_3$ additive was used as electrolyte. The specific capacity of Li-S battery was calculated according to the mass of sulfur. For each cell, the electrolyte/sulfur (E/S) usage ratio is controlled at around 12 μL mg^{-1} for the low sulfur loading electrode (1.6 mg cm^{-2}). For high sulfur loading of 3.3, 4.6, and 6.0 mg cm^{-2}, E/S ratio of 7.7, 5.5, and 4.2 μL mg^{-1} were applied, respectively. 3.7 μL mg^{-1} E/S ratio was applied for the electrode with higher sulfur loading of 10.3 mg cm^{-2}. The Li//Li symmetric cells were assembled using Li foil as electrode with PP separator and PW_{12}-CD modified separators. For Li//Cu half cells, Cu foil was used as the working electrode and Li foil was used as the counter/reference electrode. 30 μL electrolyte was added in each cell. DH7006 electrochemical workstation (Jiangsu Donghua Analytical Instrument Co., Ltd, Donghua Analytical) was used to test CV and EIS in the

frequency range of 100 kHz~0.01 Hz with a voltage amplitude of 5 mV. The cycle performance and rate performance tests of the Li//Li and Li-S cells were carried out on the Neware battery test system (CT-4008-5V50mA-164, Shenzhen Neware Electronics Co., Ltd., China). Li//Cu half cells were assembled to test the nucleation overpotential and Coulombic efficiency. All the above cells (CR2032) were assembled in a glove box filled up with argon (O_2 < 0.1 ppm, H_2O < 0.1 ppm).

Symmetrical cell assembly and measurement: The electrodes for symmetrical cells were prepared by mixing the as-prepared catalyst materials (CD, PW_{12}, and PW_{12}-CD), Super P, and PVDF with a weight ratio of 7:2:1 in NMP to form a slurry, and then coating them on an aluminium foil (diameter of 10 mm), which was vacuum dried at 60 °C for 12 h. 0.5 M Li_2S_6 electrolyte was prepared by mixing the S and Li_2S powder with the molar ratio of 5:1 in the mixing solvent of DOL and DME (v/v =1:1) with 1 M LiTFSI. The cyclic voltammetry (CV) profiles of symmetric cells were collected from -1.0 V to 1.0 V at scan rates of 10 mV s^{-1}. Electrochemical impedance spectroscopy (EIS) was recorded with the frequency range of 100 kHz~0.1 Hz at the open-circuit potential. The Tafel plots were recorded at a scan rate of 0.1 mV s^{-1} in the range of -0.1 V~0.1 V.

The visual adsorption and UV-vis tests: A Li_2S_6 solution was prepared through the dissolution of sulfur and Li_2S (in a 5:1 molar ratio) in a blended solvent composed of 1,2-dimethoxyethane (DME) and 1,3-dioxolane (DOL) (v/v =1:1) while vigorously stirring at a temperature of 65 ℃ for a duration of 24 h. Subsequently, 10 mg samples were added to 3 mL of 5 mM Li_2S_6 solution. Following an 8-hour immersion of the samples in the Li_2S_6 solution, ex-situ ultraviolet-visible absorption spectra were acquired.

Li_2S nucleation test: Li_2S_8 solution was prepared by mixing sulfur and Li_2S (in a 7:1 molar ratio) in the mixed solution of DOL/DME (1:1, v/v) under vigorous stirring at 65 ℃ for 12 h. The electrodes were fabricated by mixing the catalyst materials and PVDF at a weight ratio of

9:1 and coating them on the carbon-paper disks (diameter of 16 mm). The cells were assembled using carbon-paper loaded with the catalyst samples as the cathode, lithium foil as anode, and Celgard 2500 as the separator. 25 μL Li_2S_8 solution was added on the cathode side and 25 μL blank electrolyte was added on the anode side. The cells were discharged galvanostatically at 0.112 mA to 2.10 V and then kept potentiostatically at 2.08 V for Li_2S to nucleate and grow until current dropped below 10^{-5} A. It took about 60,000 s and the capacity of Li_2S conversion could be evaluated based on the quantity of electric charge according to Faraday's law.

Linear sweep-voltammetry (LSV) measurements: Three-electrode LSV tests were performed to evaluate the catalytic activity of the samples for Li_2S oxidation. The preparation of working electrodes was the same as that of symmetric cells. The counter electrode and reference electrode were respectively platinum wire and saturated Ag/AgCl electrode. 0.1 M Li_2S dissolved in methanol solution was used as electrolyte. The LSV curves were measured at a scanning rate of 50 mV s^{-1} from -0.5 V to -0.1 V.

Shuttle current measurements: The assembled cells were discharged and charged three times at 0.05 C to ensure complete transition of S in the cathode, and then discharged to 2.25 V *versus* Li/Li^+, at which most of the S was converted to long chain polysulfides (Li_2S_8 and Li_2S_6). The open circuit voltage (OCV) was then measured. The OCV was applied and held to the external circuit and the current was recorded. The current in the steady state can be considered as the shuttle current. Note that the electrolyte is $LiNO_3$ free.

Part of the formula: The ionic conductivity (σ) of the electrolyte-soaked separators was evaluated with two stainless steel (SS) blocking cells (SS//separator//SS) by testing the EIS in the frequency range from 1000 kHz to 0.01 Hz on the electrochemical workstation. The ionic conductivity was calculated according to the following equation:

$$\sigma = \frac{d}{R_b S} \tag{S1}$$

where d is the thickness of the separator, R_b and S represent the bulk resistance and the effective area of the separator, respectively.

R_0 and R_s refer to the interfacial resistance before and after AC impedance. I_0 and I_s represent the current value in initial and steady state under a polarization potential of 10 mV. t_{Li^+} is the lithium transfer number, and the value is calculated as follows.

$$t_{Li}{}^{+} = \frac{I_s(\Delta V - I_0 R_0)}{I_0(\Delta V - I_s R_s)} \tag{S2}$$

The t_{Li^+} is largely enhanced, which prolongs the "Sand's time" of lithium dendrites nucleation according to Sand's formula as described below:

$$t_{Sand} = \pi D_{app} \frac{(Z_c C_0 F)^2}{4(J t_a)^2} \tag{S3}$$

where D_{app} represents the apparent diffusion coefficient, Z_c is the charge number of the cation (Z_c = 1 for Li^+), C_0 is the bulk salt concentration, F and J are Faraday's constant and the current density, respectively, and t_a is the transference number of anions.

DFT calculations: The calculations were performed within the framework of DFT, by using the projector augmented wave method as implemented in the Vienna ab Initio Simulation Package. The exchange-correlation energy was in the form of Perdew-Bruke-Ernzerhof. The cutoff energy for the plane-wave basis set was 500 eV, and 2×2×1 Γ-centered k-point grids were used for the Brillouin zone integrations. For the surface systems, the bottom atom layers were fixed to simulate the body state, while the top atom layers were free to simulate the surface state. To reduce the interactions between each surface, a vacuum of 20 Å was contained in our calculation models. All structures were fully relaxed to the optimized geometry with the force convergence set at 0.01 eV/Å. To investigate the lowest energy configurations of adsorbed systems, we carefully manipulated structure parameters of the initial state (the distance, angle, and displacement between molecule and surface) to fully relax and selected the lowest energy

result as the final state. The binding energy (E_{ads}) of LPSs adsorbing on the CD or PW_{12} is calculated referring to the following equation:

$$E_{ads} = E_{total} - E_{CD/PW12} - E_{LPSs} \quad \text{(S4)}$$

where E_{total} is the total energy of CD or PW_{12} combined with LPSs, $E_{CD/PW12}$ is the surface energy of CD or PW_{12}, and E_{LPSs} represents the energy of LPSs in vacuum.

2. Supporting Figures

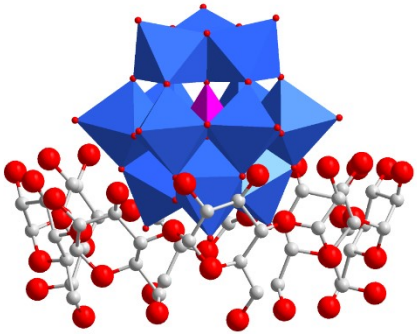

Fig. S1. Structural representation of crystalline PW_{12}-CD. (Color code: W, dark blue; P, lavender; O, red; C, gray)

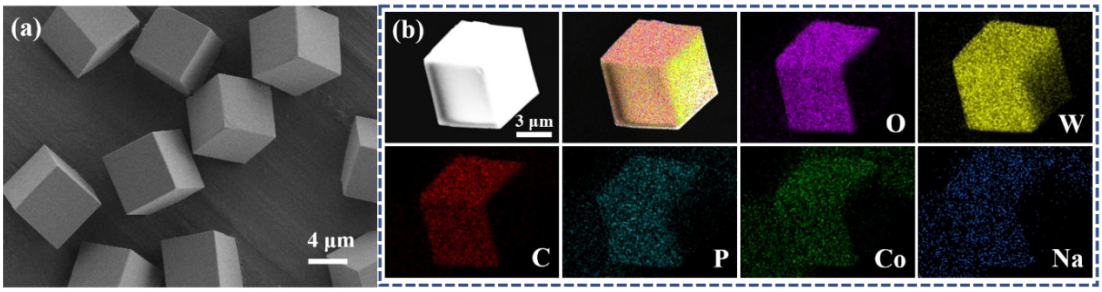

Fig. S2. SEM image and mapping images of the synthesised PW_{12}-CD crystalline material.

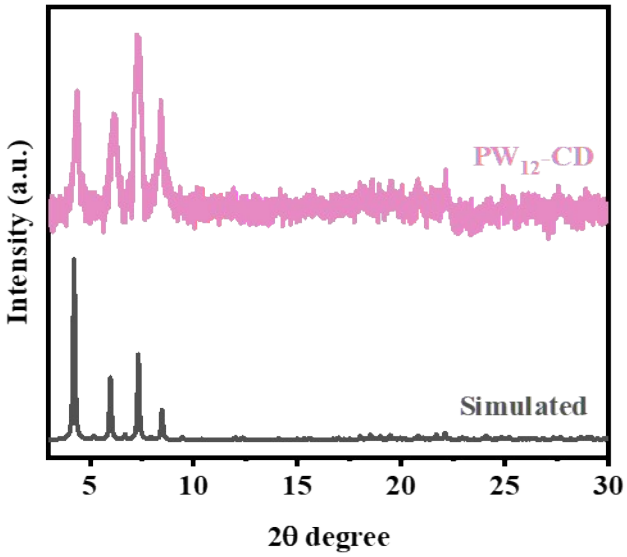

Fig. S3. Experimental and simulated XRD patterns of PW_{12}-CD.

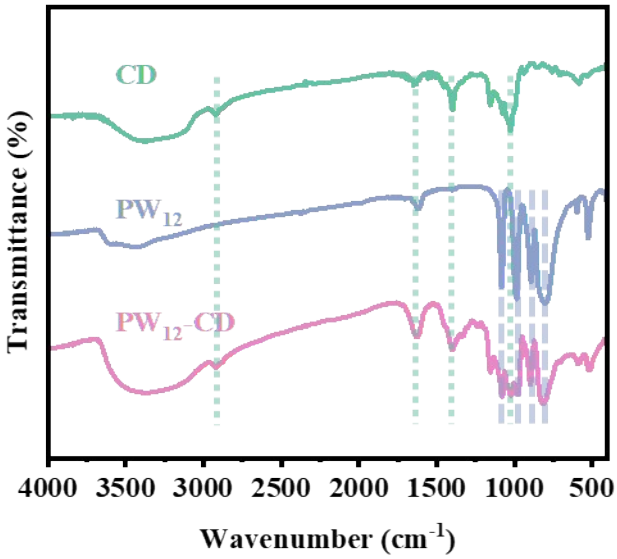

Fig. S4. FTIR spectra of CD, PW_{12}, and PW_{12}-CD.

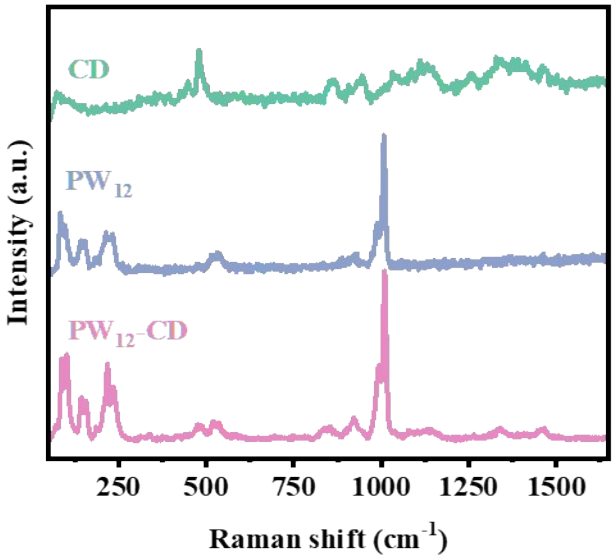

Fig. S5. Raman spectra of CD, PW_{12}, and PW_{12}-CD.

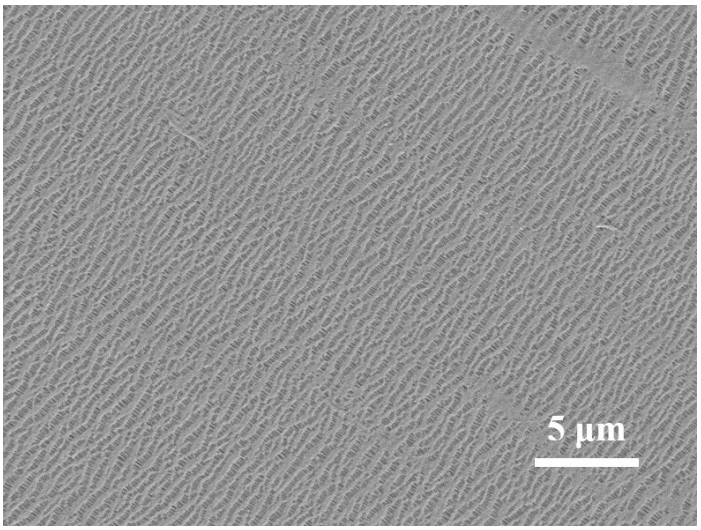

Fig. S6. The top surface SEM image of pristine sepatator.

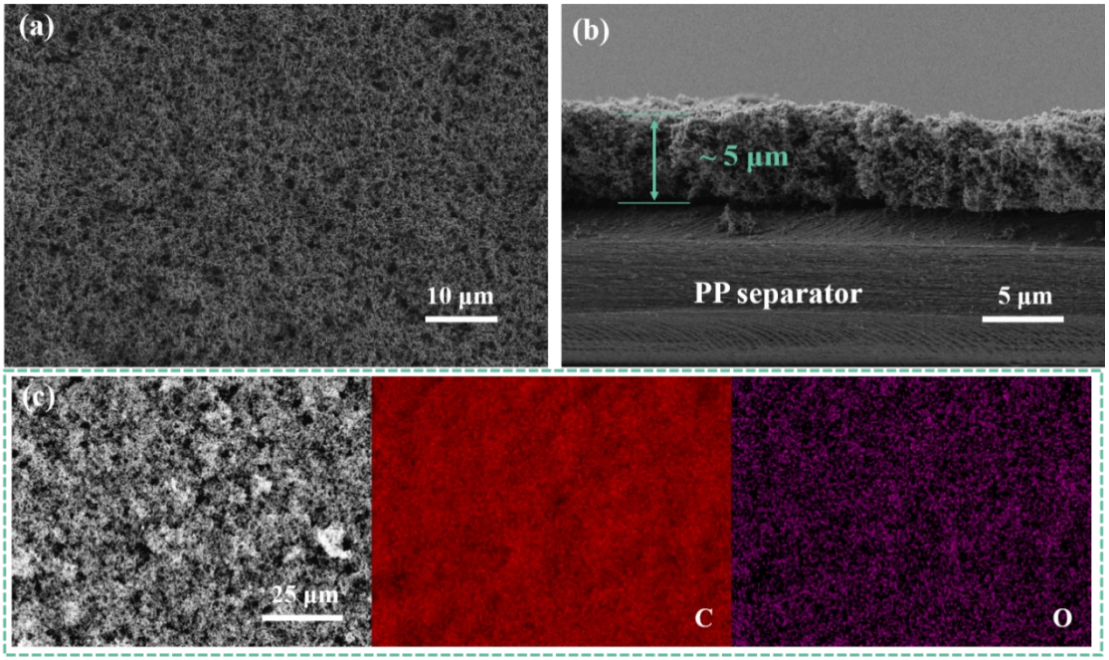

Fig. S7. (a) The top surface and (b) cross section SEM images of CD modified sepatator. (c) The element mapping images of CD modified sepatator.

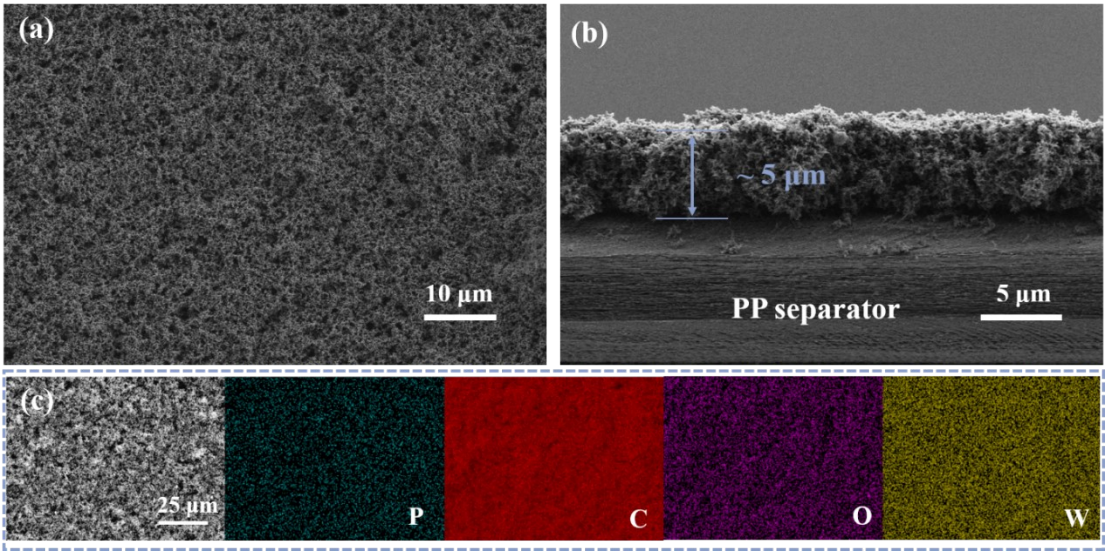

Fig. S8. (a) The top surface and (b) cross section SEM images of PW_{12} modified sepatator. (c) The element mapping images of PW_{12} modified sepatator.

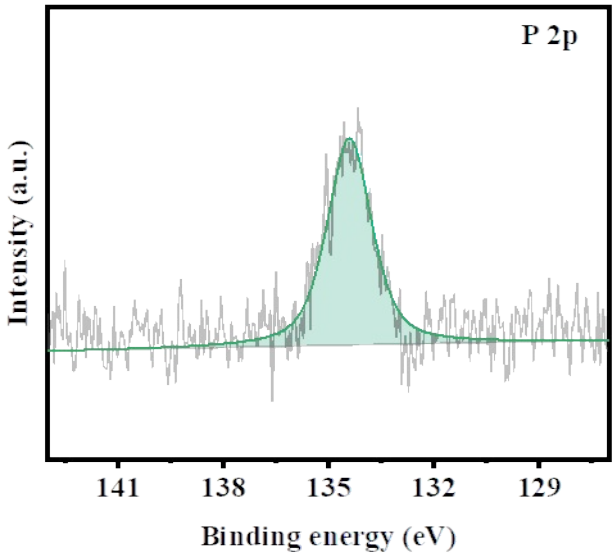

Fig. S9. P 2p XPS spectra of PW_{12}-CD modified separator.

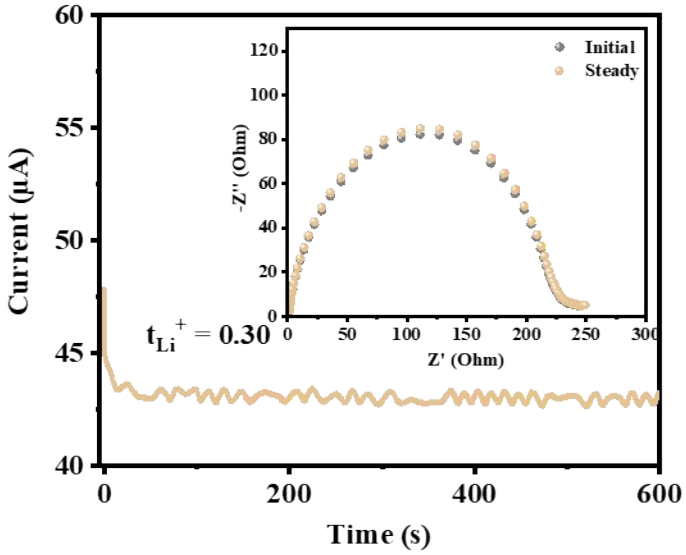

Fig. S10. Measurement of t_{Li}^{+} using potentiostatic polarization of Li//Li symmetric cell with pristine PP separator (inset: Nyquist plots of impedance before and after polarization).

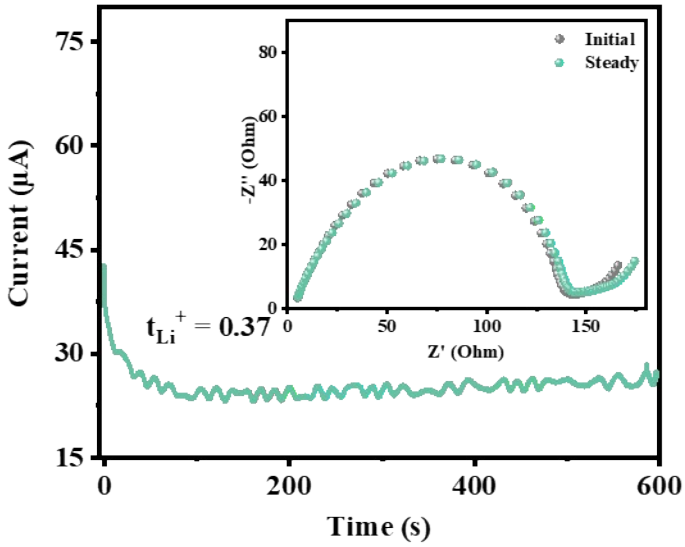

Fig. S11. Measurement of t_{Li}^{+} using potentiostatic polarization of Li//Li symmetric cell with CD modified separator (inset: Nyquist plots of impedance before and after polarization).

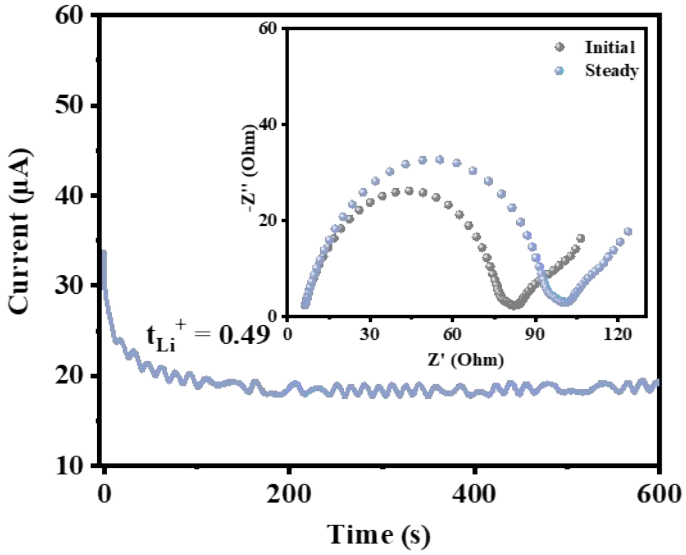

Fig. S12. Measurement of t_{Li}^{+} using potentiostatic polarization of Li//Li symmetric cell with PW_{12} modified separator (inset: Nyquist plots of impedance before and after polarization).

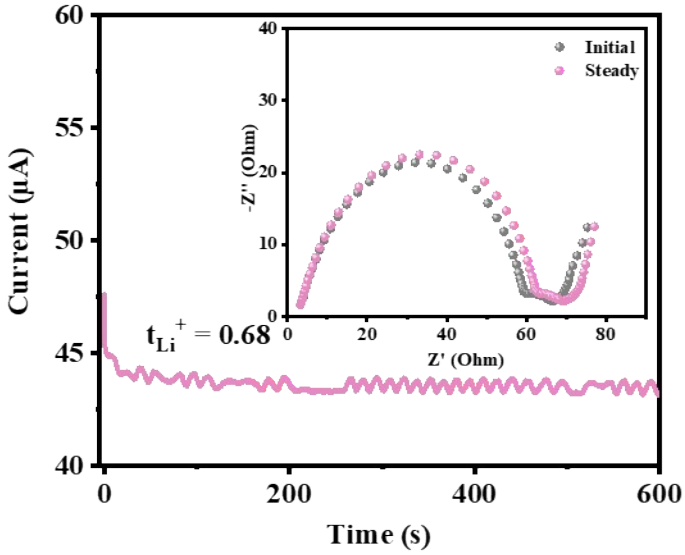

Fig. S13. Measurement of t_{Li}^{+} using potentiostatic polarization of Li//Li symmetric cell with PW_{12}-CD modified separator (inset: Nyquist plots of impedance before and after polarization).

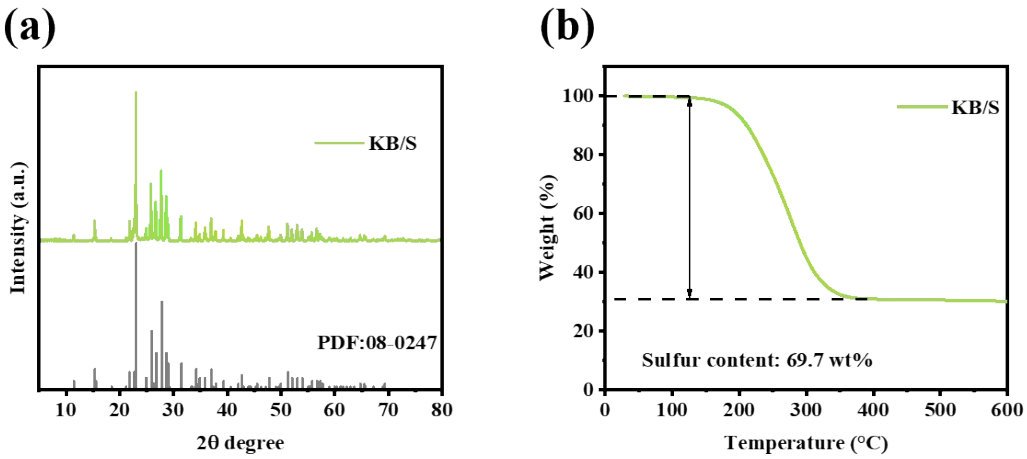

Fig. S14. (a) XRD pattern and (b) TGA curve of KB/S.

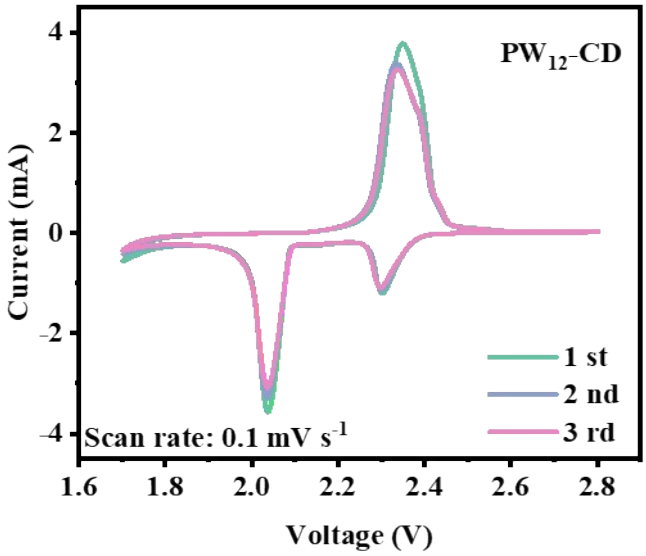

Fig. S15. CV curves of the Li-S cell with PW_{12}-CD modified separator at a scan speed of 0.1 mV s^{-1}.

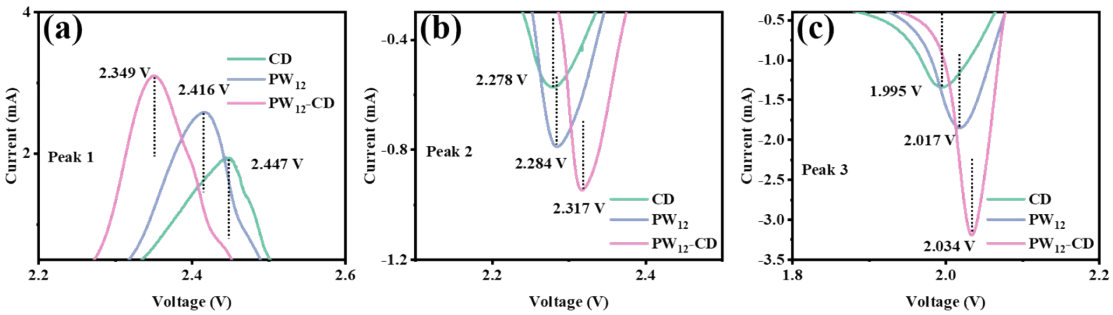

Fig. S16. CV profiles of the enlarged view in peak 1 (a), peak 2 (b), and peak 3 (c).

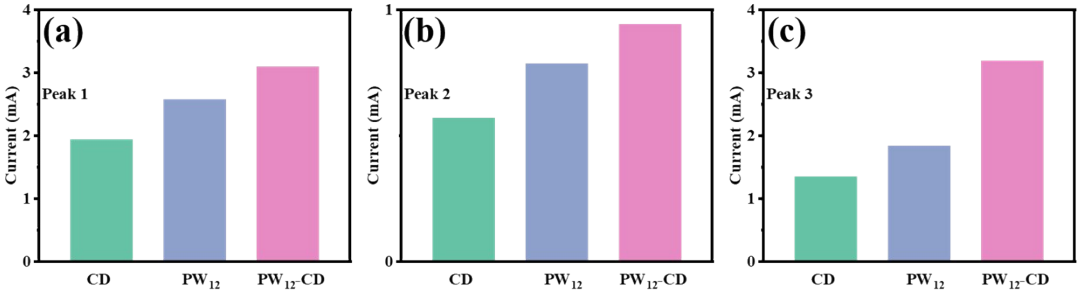

Fig. S17. Peak current of peak 1 (a), peak 2 (b), and peak 3 (c).

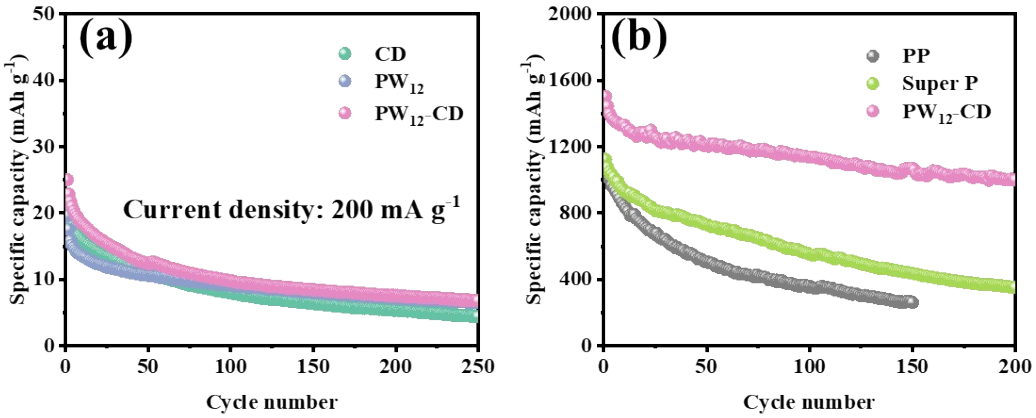

Fig. S18. (a) Cycle performance of the cells with CD, PW_{12}, and PW_{12}-CD electrodes at the current density of 200 mA g^{-1} in the voltage range of 1.7-2.8 V. The electrode is composed of 70% active materials (CD, PW_{12} or PW_{12}-CD), 20% Super P, and 10% PVDF by weight. The electrolyte used here is the same as the Li-S cells. (b) Cycle performance of the cells with PW_{12}-CD modified separator, bare Super P modified separator, and pristine PP separator at 0.1 C.

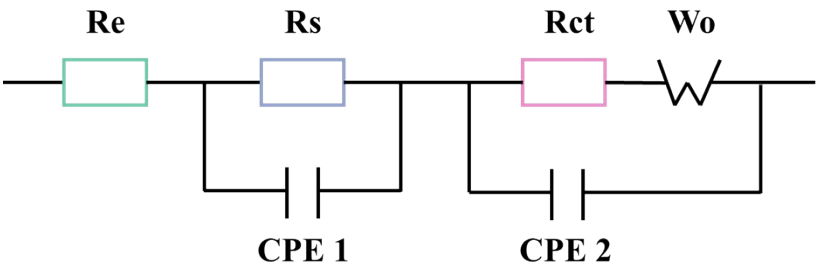

Fig. S19. The equivalent circuit used to simulate EIS curves.

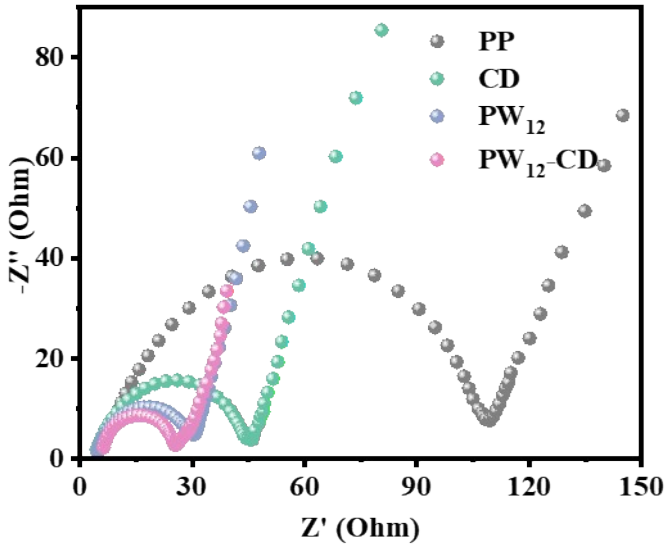

Fig. S20. Nyquist curves of Li-S cells with different separators before cycling.

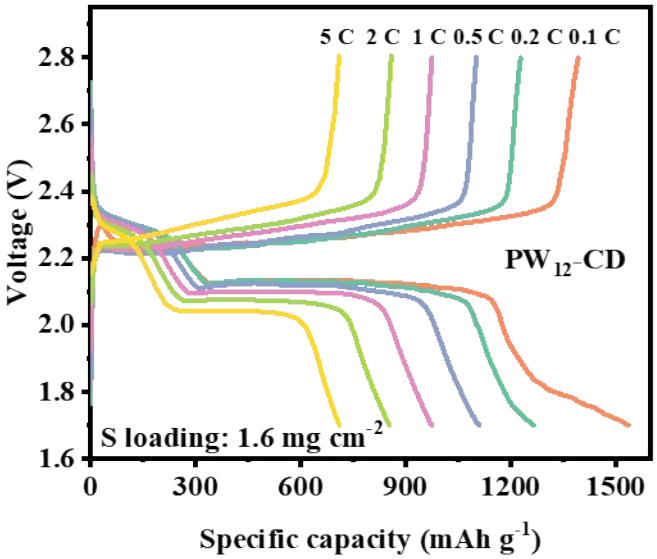

Fig. S21. Galvanostatic charge-discharge curves of Li-S cells based on PW_{12}-CD modified separator under different C-rates.

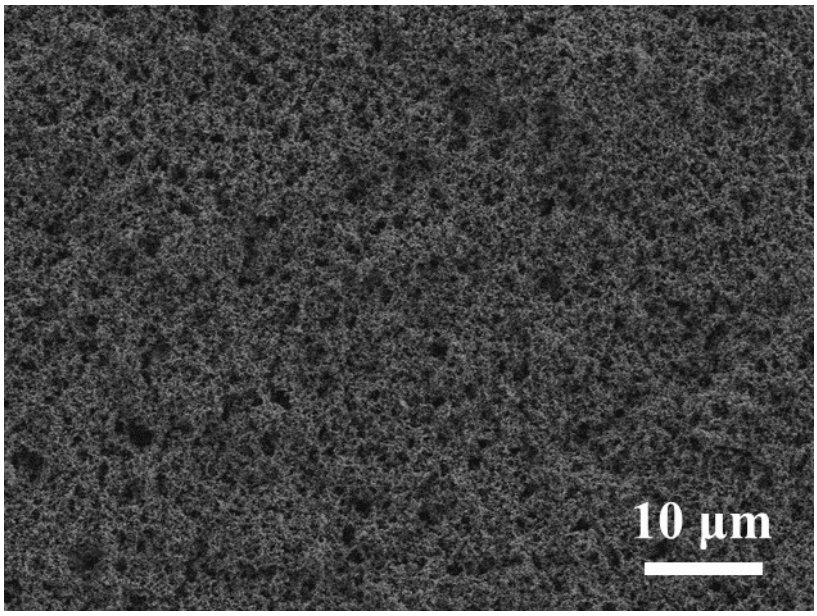

Fig. S22. SEM image of PW_{12}-CD modified separator after cycles.

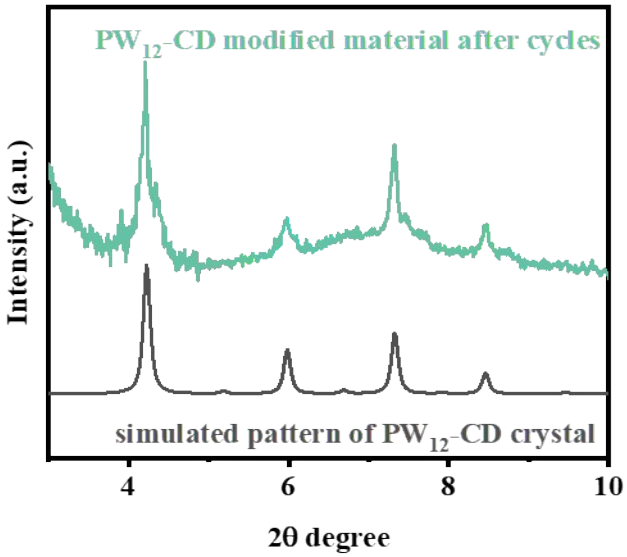

Fig. S23. XRD pattern of PW_{12}-CD modified material after cycles.

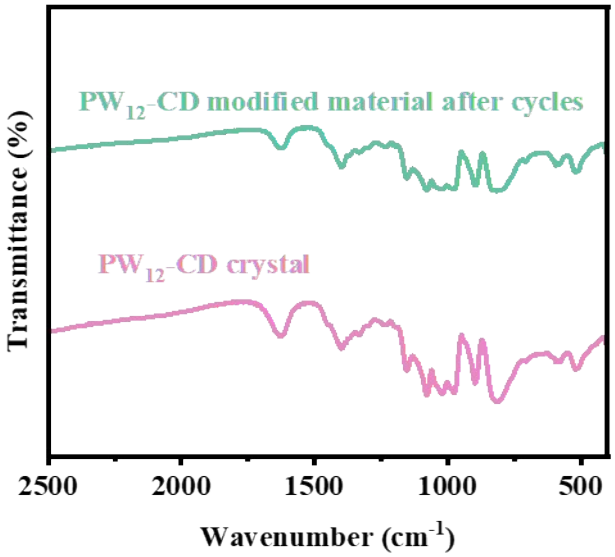

Fig. S24. FTIR spectra of PW_{12}-CD crystal and PW_{12}-CD modified material after cycles.

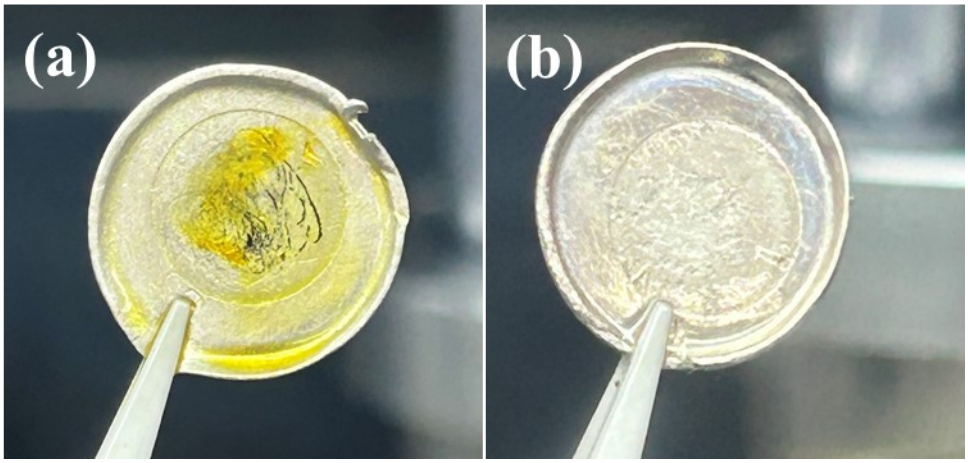

Fig. S25. The optical photographs of lithium metal electrodes for the cells with (a) PP separator and (b) PW_{12}-CD modified separator after cycles.

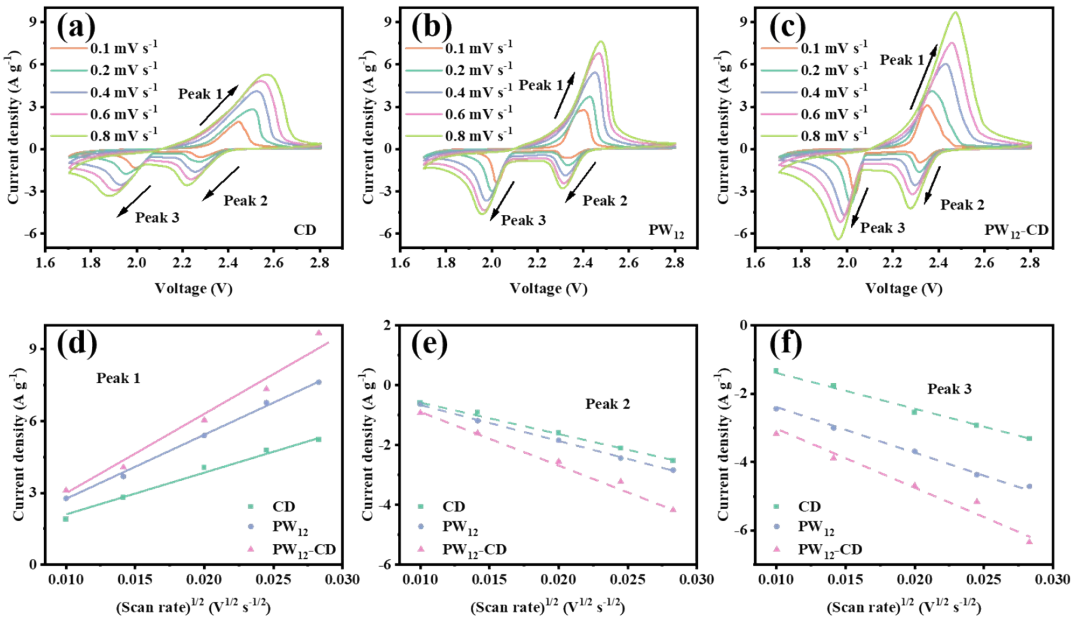

Fig. S26. CV profiles of the cells with (a) CD, (b) PW_{12}, and (c) PW_{12}-CD modified separators at various scan rates from 0.1 mV s^{-1} to 0.8 mV s^{-1}; (d-f) Plots of peak current *vs.* square root of scan rates for the cells with CD, PW_{12}, and PW_{12}-CD modified separators.

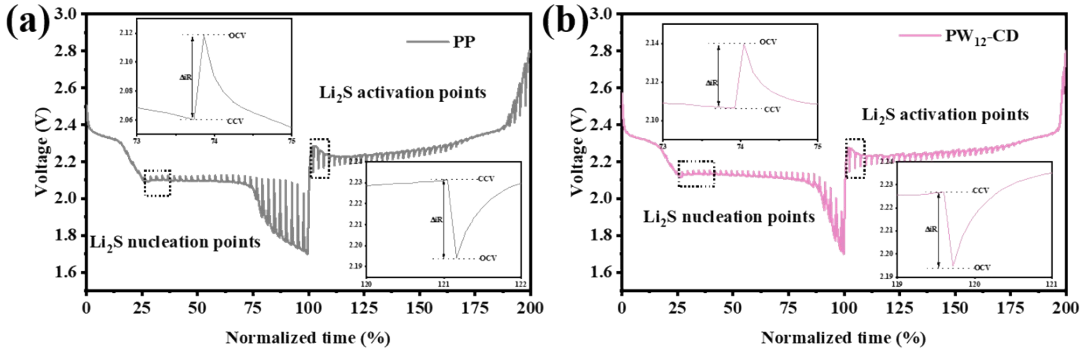

Fig. S27. GITT plots of Li-S cells with (a) PP separator and (b) PW_{12}-CD modified separator at a current density of 0.2 C.

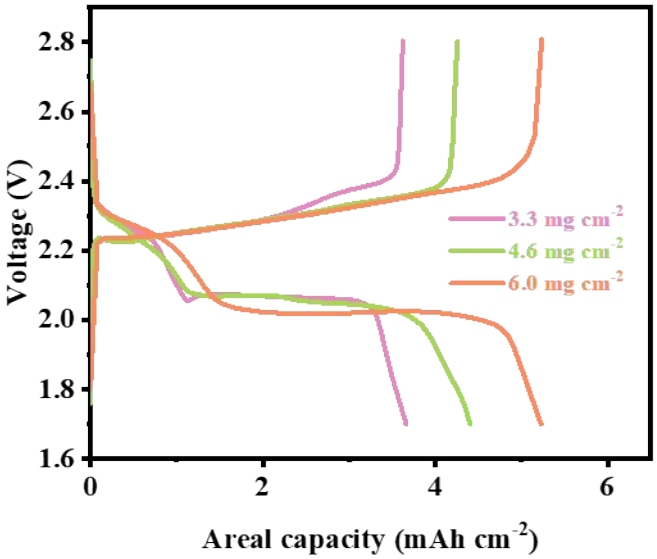

Fig. S28. Galvanostatic charge-discharge profiles of Li-S cells with PW_{12}-CD modified separator under different sulfur loadings.

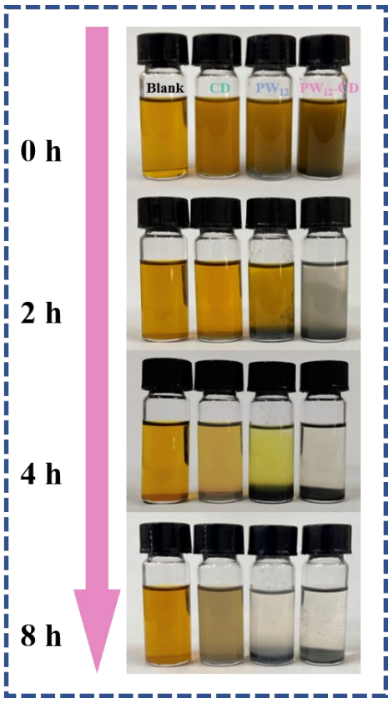

Fig. S29. Optical observation of Li_2S_6 solution adsorbed by CD, PW_{12}, and PW_{12}-CD.

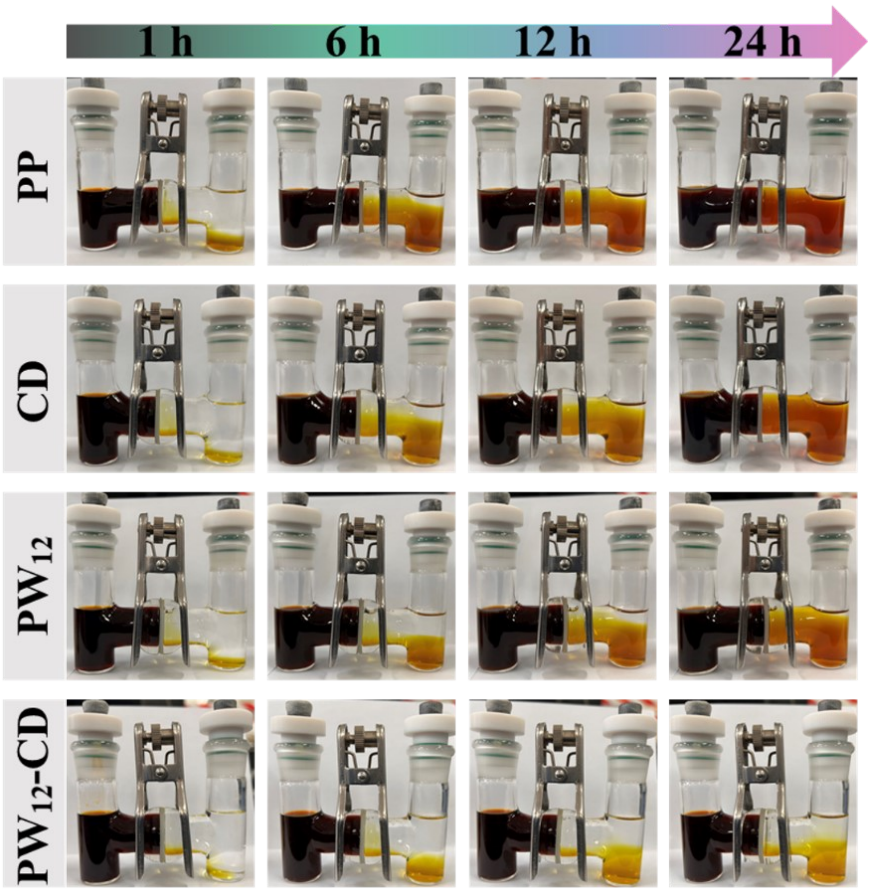

Fig. S30. The penetration test with the pristine PP separator, CD, PW_{12}, and PW_{12}-CD modified separators.

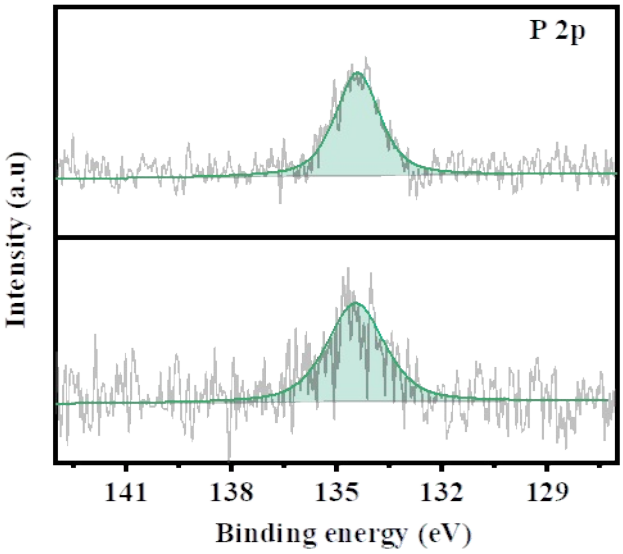

Fig. S31. P 2p spectra for PW_{12}-CD and PW_{12}-CD@Li_2S_6.

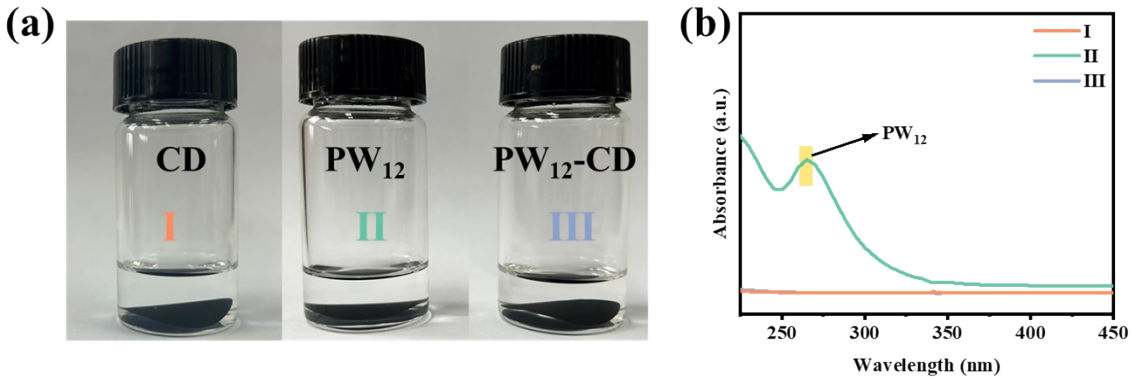

Fig. S32. (a) Observation of solubility of CD, PW_{12}, and PW_{12}-CD modified separators in 5 mL DME electrolyte. (b) Corresponding UV-vis spectra of the supernatant.

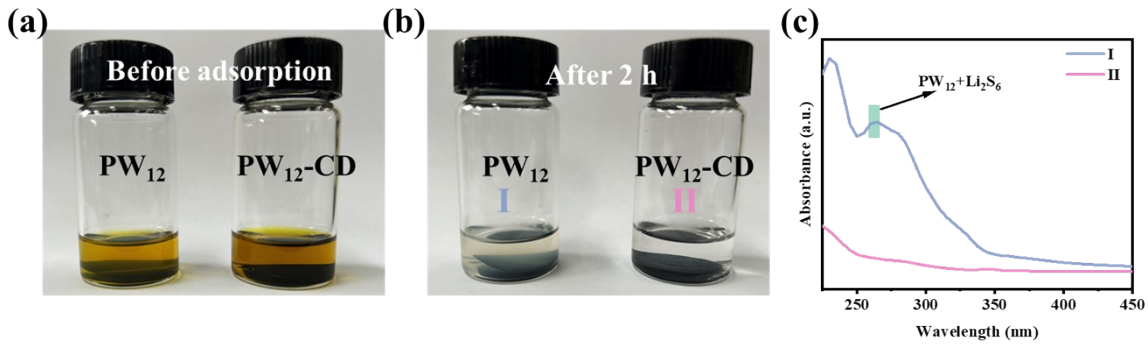

Fig. S33. Observation of solubility of PW_{12} and PW_{12}-CD modified separators in (a) 5 mL DME with Li_2S_6 and (b) 5 mL DME with Li_2S_6 for 2 h. (c) Corresponding UV-vis spectra of the supernatant.

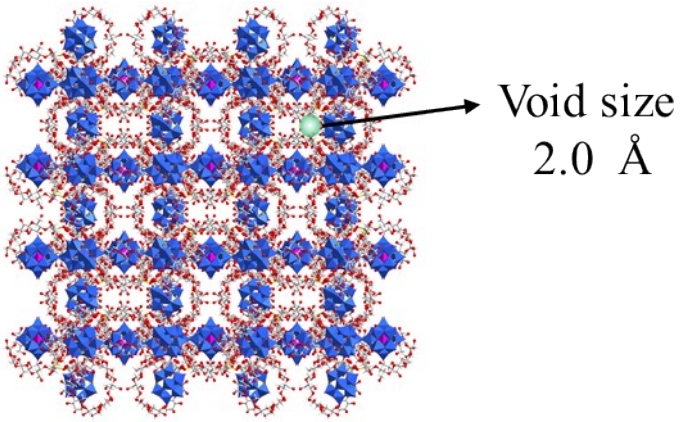

Fig. S34. Stacking pattern of crystalline PW_{12}-CD. (Color code: W, dark blue; P, lavender; O, red; C, gray)

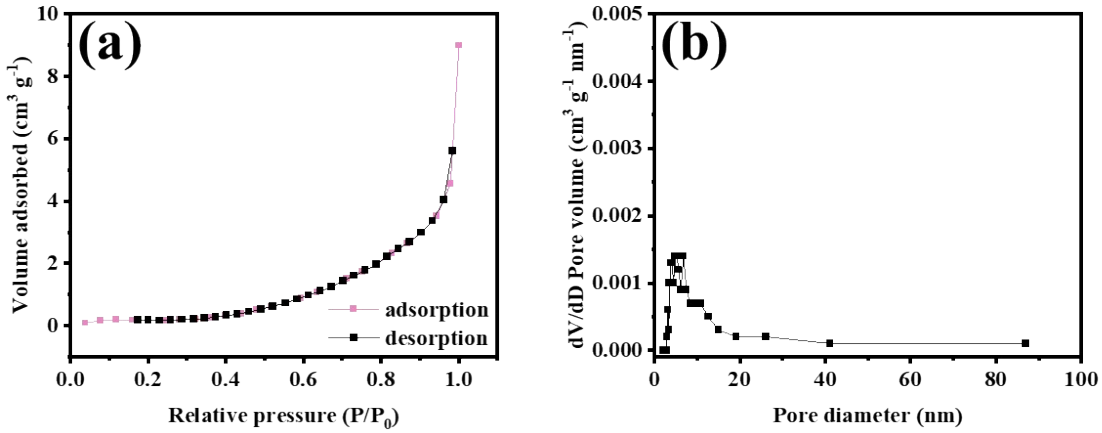

Fig. S35. (a) N_2 adsorption-desorption isotherms for PW_{12}-CD complex. (b) Corresponding pore size distribution.

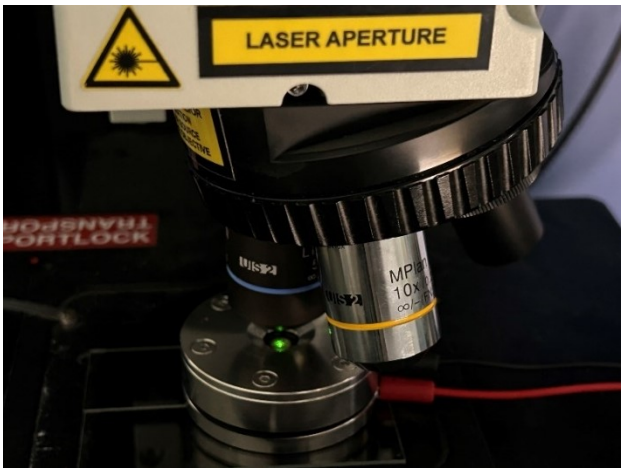

Fig. S36. Digital photographs of an in-situ Raman equipment.

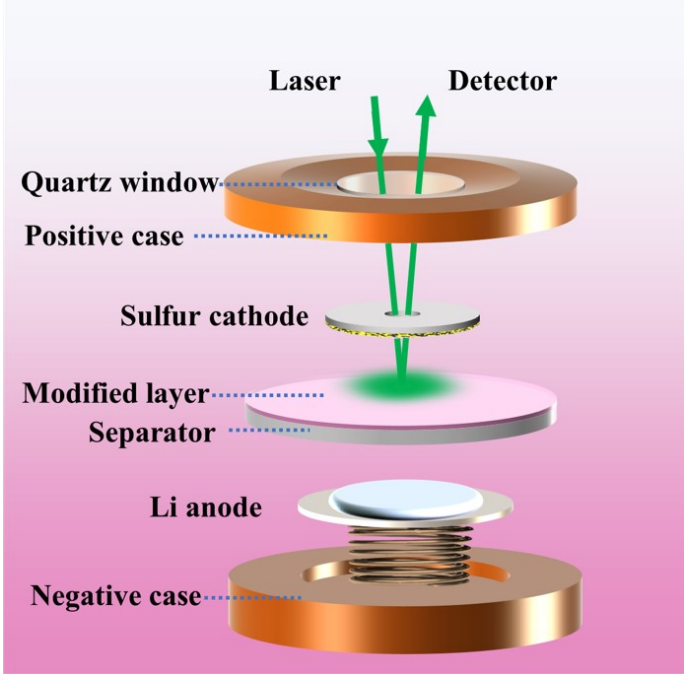

Fig. S37. Schematic illustration of a Li-S cell toward in-situ Raman tests.

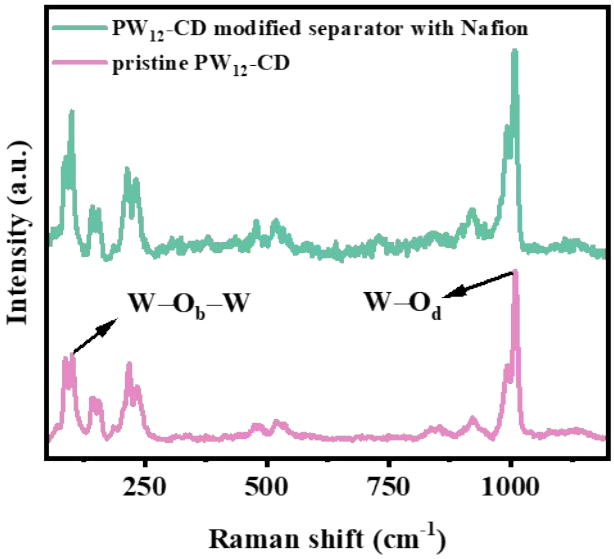

Fig. S38. Raman spectra of pristine PW_{12}-CD and PW_{12}-CD modified separator with Nafion.

Table S1. Electrochemical performance comparison of Li-S cell with PW_{12}-CD modified separator and other modified separators in recent literatures (sulfur loading ≤ 2 mg cm^{-2}).

Modified materials	Sulfur loading (mg cm^{-2})	Current density (C)	Initial capacity (mAh g^{-1})	Discharge capacity (mAh g^{-1}) after n^{th} cycle	Capacity decay rate (per cycle)	Ref.
PW_{12}-CD	1.6	1	1091	828 (1000^{th})	0.024 %	This work
PW_{12}-CD	1.6	2	956	732 (1000^{th})	0.023 %	
AlMMT-SP	1.0-1.2	1	1070	625 (1000^{th})	0.042 %	[2]
$Ti_3C_2T_x$-CNT	0.9	1	-	535 (500^{th})	0.070 %	[3]
LDH@NG	1.2	2	812	373 (1000^{th})	0.060 %	[4]
$Se_{0.06}$SPAN/MMT@PP	0.8	1	1200	784 (1000^{th})	0.034 %	[5]
AAPP/CB@PP@LAGP	1.0-1.2	1	1045	700 (500^{th})	0.065 %	[6]
$Ti_3C_2T_x$/Ni-Co MOF@PP	1.5	1	910	682 (500^{th})	0.046 %	[7]
ZIF-67/SA-PAN	1.0	1	801	445 (500^{th})	0.089 %	[8]
FeSC@NSC	1.5-2.0	1	852	466 (700^{th})	0.064 %	[9]
FeSC@NSC	1.5-2.0	2	640	415 (700^{th})	0.050 %	[9]

Table S2. The reactions occurred on working and counter electrodes in Li_2S_6 symmetric cell.

Peak	Working electrode	Counter electrode
a	$S_6^{2-} + 10e^- + 12Li^+ \rightarrow 6Li_2S$	$4S_6^{2-} - 8e^- \rightarrow 3S_8$
b	$6Li_2S - 10e^- \rightarrow S_6^{2-} + 12Li^+$	$3S_8 + 8e^- \rightarrow 4S_6^{2-}$
c	$4S_6^{2-} - 8e^- \rightarrow 3S_8$	$S_6^{2-} + 10e^- + 12Li^+ \rightarrow 6Li_2S$
d	$3S_8 + 8e^- \rightarrow 4S_6^{2-}$	$6Li_2S - 10e^- - 12Li^+ \rightarrow S_6^{2-}$

Table S3. Electrochemical performance comparison of Li-S cell with PW_{12}-CD modified separator and other modified separators in recent literatures (sulfur loading ≥ 5 mg cm^{-2}).

Modified materials	Modified-layer thickness (μm)	Sulfur loading (mg cm^{-2})	E/S ratio (μL mg^{-1})	Current density	Areal capacity (mAh cm^{-2})	Ref.
PW_{12}-CD	5	10.3	3.7	0.2 C	7.9	This work
AlMMT-SP	12	6.1	5	0.05 C	5.0	[2]
Sb_2Se_{3-x}/rGO	32	8.1	10	0.1 C	7.46	[10]
InN	6.5	6.0	20	0.1 C	5.71	[11]
$NiCo_2O_4$@rGO	9.6	6.0	10	0.1 C	5.03	[12]
Pt SAs/In_2S_3/Ti_3C_2	8.5	6.4	10	0.2 C	5.54	[13]
sCAP	6	6.8	5.6	0.2 C	5.9	[14]
SCOF-2	6	8.2	5	0.1 C	6.1	[15]
RG@CoS@C	30	5	8.1	0.2 C	4	[16]

References

[1] Z. G. Jiang, W. T. Mao, D. P. Huang, Y. Wang, X. J. Wang and C. H. Zhan, A nonconventional host-guest cubic assembly based on gamma-cyclodextrin and a Keggin-type polyoxometalate, *Nanoscale*, 2020, **12**, 10166-10171.

[2] Y. Wang, Y. Wu, P. Mao, Y. Fan, X. Wang, H. Xiang, Z. Li, K. Li and C. Hu, A Keggin Al(13) -Montmorillonite Modified Separator Retards the Polysulfide Shuttling and Accelerates Li-Ion Transfer in Li-S Batteries, *Small*, 2024, **20**, 2304898.

[3] D. Xiong, S. Huang, D. Fang, D. Yan, G. Li, Y. Yan, S. Chen, Y. Liu, X. Li, Y. Von Lim, Y. Wang, B. Tian, Y. Shi and H. Y. Yang, Porosity Engineering of MXene Membrane towards Polysulfide Inhibition and Fast Lithium Ion Transportation for Lithium-Sulfur Batteries, *Small*, 2021, **17**, 2007442.

[4] H. J. Peng, Z. W. Zhang, J. Q. Huang, G. Zhang, J. Xie, W. T. Xu, J. L. Shi, X. Chen, X. B. Cheng and Q. Zhang, A Cooperative Interface for Highly Efficient Lithium-Sulfur Batteries, *Adv. Mater.*, 2016, **28**, 9551-9558.

[5] W. Wang, K. Xi, B. Li, H. Li, S. Liu, J. Wang, H. Zhao, H. Li, A. M. Abdelkader, X. Gao and G. Li, A Sustainable Multipurpose Separator Directed Against the Shuttle Effect of Polysulfides for High-Performance Lithium–Sulfur Batteries, *Adv. Energy Mater.*, 2022, **12**, 202200160.

[6] C. Ma, Y. Feng, X. Liu, Y. Yang, L. Zhou, L. Chen, C. Yan and W. Wei, Dual-engineered separator for highly robust, all-climate lithium-sulfur batteries, *Energy Storage Mater.*, 2020, **32**, 46-54.

[7] Y. Ren, Q. Zhai, B. Wang, L. Hu, Y. Ma, Y. Dai, S. Tang and X. Meng, Synergistic Adsorption-Electrocatalysis of 2D/2D heterostructure toward high performance Li-S batteries, *Chem. Eng. J.*, 2022, **439**, 135535.

[8] Z. Li, Y. Sun, X. Wu, H. Yuan, Y. Yu and Y. Tan, Boosting Adsorption and Catalysis of Polysulfides by Multifunctional Separator for Lithium–Sulfur Batteries, *ACS Energy Lett.*, 2022, **7**, 4190-4197.

[9] X. Zuo, M. Zhen, D. Liu, H. Yu, X. Feng, W. Zhou, H. Wang and Y. Zhang, A Multifunctional Catalytic Interlayer for Propelling Solid–Solid Conversion Kinetics of Li_2S_2 to Li_2S in Lithium–Sulfur Batteries, *Adv. Funct. Mater.*, 2023, **33**, 2214206.

[10] Y. Tian, G. Li, Y. Zhang, D. Luo, X. Wang, Y. Zhao, H. Liu, P. Ji, X. Du, J. Li and Z. Chen, Low-Bandgap Se-Deficient Antimony Selenide as a Multifunctional Polysulfide Barrier toward High-Performance Lithium-Sulfur Batteries, *Adv. Mater.*, 2020, **32**, e1904876.

[11] L. Zhang, X. Chen, F. Wan, Z. Niu, Y. Wang, Q. Zhang and J. Chen, Enhanced Electrochemical Kinetics and Polysulfide Traps of Indium Nitride for Highly Stable Lithium-Sulfur Batteries, *ACS Nano*, 2018, **12**, 9578-9586.

[12] X. Lv, T. Lei, B. Wang, W. Chen, Y. Jiao, Y. Hu, Y. Yan, J. Huang, J. Chu, C. Yan, C. Wu, J. Wang, X. Niu and J. Xiong, An Efficient Separator with Low Li-Ion Diffusion Energy Barrier Resolving Feeble Conductivity for Practical Lithium–Sulfur Batteries, *Adv. Energy Mater.*, 2019, **9,** 1901800.

[13] C. Zhou, M. Li, N. Hu, J. Yang, H. Li, J. Yan, P. Lei, Y. Zhuang and S. Guo, Single-Atom-Regulated Heterostructure of Binary Nanosheets to Enable Dendrite-Free and Kinetics-Enhanced Li–S Batteries, *Adv. Funct. Mater.*, 2022, **32**, 2204635.

[14] Y.-H. Liu, W. Chang, J. Qu, Y.-Q. Sui, Y. Abdelkrim, H.-J. Liu, X.-Z. Zhai, Y.-G. Guo and Z.-Z. Yu, A polymer organosulfur redox mediator for high-performance lithium-sulfur batteries, *Energy Storage Mater.*, 2022, **46**, 313-321.

[15] J. Xu, S. An, X. Song, Y. Cao, N. Wang, X. Qiu, Y. Zhang, J. Chen, X. Duan, J. Huang, W. Li and Y. Wang, Towards High Performance Li-S Batteries via Sulfonate-Rich COF-Modified Separator, *Adv. Mater.*, 2021, **33**, e2105178.

[16]J. Guo, H. Jiang, X. Li, Z. Chu, W. Zheng, Y. Dai, X. Jiang, X. Wu and G. He, Defective graphene coating-induced exposed interfaces on CoS nanosheets for high redox electrocatalysis in lithium-sulfur batteries, *Energy Storage Mater.*, 2021, **40**, 358-367.